Occurrence of a high-temperature superconducting phase in $(CaCuO_2)_n/(SrTiO_3)_m$ superlattices

D. Di Castro,[1] M. Salvato,[2] A. Tebano,[1] D. Innocenti,[1] C. Aruta,[3] W. Prellier,[4] O. I. Lebedev,[4] I. Ottaviani,[2] N. B. Brookes,[5] M. Minola,[6] M. Moretti Sala,[5,6] C. Mazzoli,[6] P. G. Medaglia,[7] G. Ghiringhelli,[6] L. Braicovich,[6] M. Cirillo,[2] and G. Balestrino[1]

[1]*CNR-SPIN and Dipartimento di Ingegneria Civile e Ingegneria Informatica, Università di Roma Tor Vergata, Via del Politecnico 1, I-00133 Roma, Italy*

[2]*Dipartimento di Fisica and MINAS Lab., Università di Roma Tor Vergata, I-00133 Roma, Italy*

[3]*CNR-SPIN, Dipartimento di Scienze Fisiche, Via Cintia, Monte S. Angelo, 80126 Napoli, Italy*

[4]*Laboratoire CRISMAT, UMR 6508, CNRS-ENSICAEN 6Bd Marechal Juin, 14050 Caen, France*

[5]*European Synchrotron Radiation Facility, 6 rue Jules Horowitz, BP 220, 38043 Grenoble, Cedex 9, France*

[6]*CNISM and Dipartimento di Fisica, Politecnico di Milano, I-20133, Italy*

[7]*CNR-SPIN and Dipartimento di Ingegneria Industriale, Università di Roma Tor Vergata, Via del Politecnico 1, I-00133 Roma, Italy*

(Received 13 March 2012; revised manuscript received 8 October 2012; published 22 October 2012)

We report the occurrence of superconductivity, with maximum $T_c = 40$ K, in superlattices (SLs) based on two insulating oxides, namely $CaCuO_2$ and $SrTiO_3$. In these $(CaCuO_2)_n/(SrTiO_3)_m$ SLs, the CuO_2 planes belong only to $CaCuO_2$ block, which is an antiferromagnetic insulator. Superconductivity, confined within a few unit cells at the $CaCuO_2/SrTiO_3$ interface, shows up only when the SLs are grown in a highly oxidizing atmosphere, because of extra oxygen ions entering at the interfaces. The hole doping is obtained by charge transfer from the interface layers, which thus act as charge reservoir.

DOI: 10.1103/PhysRevB.86.134524 PACS number(s): 74.78.Fk, 73.40.−c, 78.70.Dm, 81.16.Mk

I. INTRODUCTION

The parent compounds of high transition temperature (T_c) cuprate superconductors (HTS) are antiferromagnetic insulators and develop superconductivity when charge carriers are introduced in the CuO_2 planes; this injection is usually achieved by charge transfer from a properly doped structural subunit (charge reservoir). A different approach to obtain high T_c superconductivity is based on the engineering of heterostructures (HSs) or superlattices (SLs) by advanced layer by layer deposition techniques. Up to now this approach has been applied to artificial structures consisting of an insulating and a metallic cuprate, such as $CaCuO_2/BaCuO_2$[1,2] and $La_2CuO_4/La_{2-x}Sr_xCuO_4$ (LCO/LSCO).[3] In these systems the metallic cuprate acts as charge reservoir, injecting carriers in the CuO_2 planes of the insulating cuprate, thus artificially reproducing the mechanism which naturally occurs in cuprate HTS.

Bearing in mind this mechanism one could speculate about different possible choices of the charge reservoir block oxide, not necessarily a metallic cuprate. On the other hand, it has been shown that, by an adequate choice of the two constituents, it is possible to realize a metallic interface, which can be itself superconducting, as in the case of the oxide $LaAlO_3/SrTiO_3$ HS,[4] semiconducting monochalcogenide HSs,[5] bicrystals of semimetals[6] and multigraphene.[7]

This extraordinary interface phenomenon suggests that it could be possible to identify two systems, one copper oxide and one copper-free oxide, in order to obtain a doped interface, which could act as charge reservoir for the cuprate block. Following this idea we have chosen two insulating oxides, the $SrTiO_3$ (STO) and the $CaCuO_2$ (CCO), as building blocks for the engineering of $(CCO)_n/(STO)_m$ SLs, where n and m are the number of unit cells (u.c.) of CCO and STO, respectively. $SrTiO_3$ is at the basis of the emerging field of oxide electronics because of the occurrence of exotic, two-dimensional phases of electron matter at the interface with other oxides.[4,8–10] $CaCuO_2$ is an antiferromagnetic insulator[11] and it is considered the simplest parent compound of HTS:[12] in this compound the CuO_2 planes, where superconductivity can occur, are separated by bare Ca atoms in a pure infinite layer (IL) structure.[11] In some IL alloys, obtained by chemical synthesis under high pressure (several GPa) conditions, superconductivity was reported[12,13] and explained by the random insertion of planar defects within the IL structure.[13,14]

In this work, we provide evidence that a high critical temperature superconducting phase, with a maximum $T_c = 40$ K, can be obtained in a controlled way by using the IL CCO and the model system STO as building blocks for the synthesis of $(CCO)_n/(STO)_m$ SL films. In these systems the superconductivity develops at the interfaces between the two constituent oxides because of the peculiar structural characteristics of the CCO/STO interfaces. These, indeed, are hybrid between the perovskite and the infinite layer structure, and thus can leave space for extra oxygen ions to come in and dope the system. The charge reservoir is likely provided by the interface layers, which inject holes in the inner CuO_2 planes of the CCO block, making the SLs superconducting, although constituted by two insulating materials. The superconducting properties of these SLs can be controlled and systematically investigated by varying the growth conditions and the relative thickness of the constituent blocks.

II. EXPERIMENTAL DETAILS

A. Sample growth

We used the pulsed laser deposition technique (KrF excimer laser = 248 nm) to synthesize several superlattice $(CCO)_n/(STO)_m$ films, made by 10 to 20 repetitions of the supercell constituted by n u.c. of CCO and m u.c. of STO. The films were deposited on 5×5 mm^2 $NdGaO_3$ (110) (NGO) oriented monocrystalline substrates obtained from Crystal, GmbH. NGO is the most suitable substrate to grow both

CCO (Ref. 15) and STO, having a pseudocubic in-plane lattice parameter ($a = 3.87$ Å) just in the middle between CCO ($a = 3.84$ Å) and STO ($a = 3.91$ Å). Two targets, with $CaCuO_2$ and $SrTiO_3$ nominal composition, mounted on a multitarget system, were used. The STO target is a commercial crystal obtained from Crystal, GmbH. The CCO target was prepared by standard solid state reaction, according to the following procedure: stoichiometric mixtures of high-purity $CaCO_3$ and CuO powders were calcined at 860 °C in air for 24 h, pressed to form a disk, and finally heated at 900 °C for 12 h. The substrate was placed at a distance 2.5 cm from the targets on a heated holder and its temperature during the deposition of the SLs was $T \simeq 600$ °C. For the growth of the superconducting SLs the deposition chamber was first evacuated down to P $\sim 10^{-5}$ mbar and then a mixture of oxygen and 12% ozone atmosphere at a pressure of about 1 mbar was used, followed by a rapid quenching in high oxygen pressure (about 1 bar). Non-superconducting SLs were grown at the same temperature and pressure but with no ozone and no high pressure quenching, as explained in the subsequent sections of the paper. NdO surface terminated NGO substrates, obtained by annealing in air at 1000 °C for 2h,[16] were also used. We found that there is no appreciable difference among samples grown on NGO with controlled and uncontrolled termination from the point of view of structural quality (as evinced from x-ray diffraction measurements) and superconducting properties.

The deposition rate of the two constituent blocks was first estimated by measuring ex-situ the thickness of single phase films of CCO and STO, grown on NGO substrate at the same growth conditions used for the SLs. The thicknesses were obtained by finite size oscillations analysis of the x-ray diffraction (XRD) spectra of the films. Afterwards, an accurate estimate of the thickness of CCO and STO within the superlattice structure was made by the analysis of the XRD spectra of the SLs. Indeed, in the XRD spectrum of a system with SL structure, as the $(CCO)_n/(STO)_m$, satellite peaks SL_{+1} and SL_{-1} show up around the average structure peak SL_0 [see Fig. 3(a)]. From the positions $2\theta_{+1}$ and $2\theta_{-1}$ of the satellite peaks [see Fig. 3(a)], it is possible to evaluate accurately the thickness of the supercell $\Lambda = n \cdot c_{CCO} + m \cdot c_{STO}$ (c_{CCO} and c_{STO} are the c-axis lattice parameters of CCO and STO, respectively), by using the following formula:[1,17] $\Lambda = \lambda/[\sin(\theta_{+1}) - \sin(\theta_{-1})]$, where λ is the wavelength of the incident radiation. From the position $2\theta_0$ of the average structure peak SL_0, the value of the mean c-axis lattice parameter $c = (n \cdot c_{CCO} + m \cdot c_{STO})/(n + m)$ is easily obtained by $c = \lambda/[2\sin(\theta_0)]$. To estimate the individual values of n and m, we synthesized several SLs $(CCO)_n/(STO)_m$ keeping fixed the number of laser shots on the STO target and varying the number N of laser shots on the CCO target. In Fig. 1 we report $\Lambda/c = n + m$, estimated by the XRD spectra as described above, as a function of the laser shots N on the CCO target for various $(CCO)_n/(STO)_m$ SLs. The value of m is kept fixed at about 2, as evaluated by the rough estimate of the deposition rate from the XRD spectra of the single phase films. The experimental points lie on a straight line, as expected if all the growth conditions (pressure, temperature, laser fluence, target to substrate distance) are not changed from one deposition to another. The extrapolation to $N = 0$ gives the thickness m (in unit cells) of the STO layer

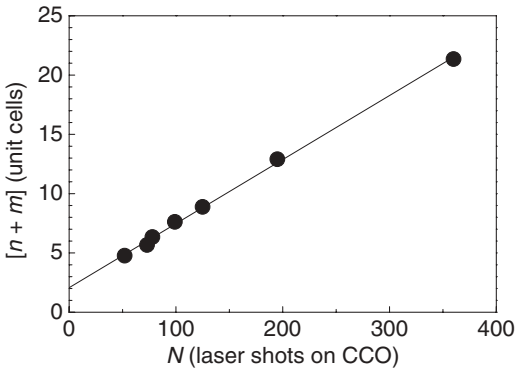

FIG. 1. Thickness of the supercell ($n + m$), in unit cells, as a function of the number N of laser shots on the CCO target. The extrapolation to $N = 0$ gives the number of unit cells of STO block.

and, consequently, the thicknesses of the CCO layer and the deposition rate of both STO and CCO. In our case, from a linear fit we obtained (approximating to half cell) $m = 2$, and thus $n = 3, 3.5, 4, 5.5, 7, 10.5, 19.5$.

B. Experimental techniques

The structural characterization was performed by x-ray diffraction measurements in a θ–2θ Bragg-Brentano geometry and by high-resolution transmission electron microscopy (HRTEM). The TEM images were taken using a Tecnai G2 30 UT microscope with a 1.7 Å point resolution, operated at 300 kV. Cross-section specimens for HRTEM were prepared by mechanically grinding down to the thickness of approximately 20 μm, followed by Ar^+ ion beam milling using a Ion Slicer EM-09100 IS apparatus. The HRTEM image simulation has been done using Mac Tempas and Cristal Kit software. A Bragg-mask filter was used in order to enhance the noise/signal ratio.

The samples for resistivity, I-V characteristics, and Hall effect measurements were patterned using a standard lithographic process in order to obtain a definite geometry. In Fig. 2 a representative picture of the patterned samples is shown. In this image, the darker area corresponds to the sample surface, with the horizontal thin strip indicated by the arrow and the position of the current and voltage terminals indicated by I and V, respectively.

In the case of the I-V measurements the strip width was w = 90 μm and the distance between the in-line voltage

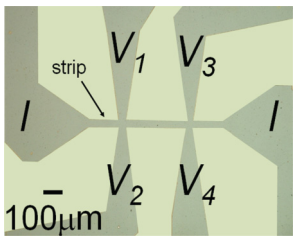

FIG. 2. (Color online) Representative picture of a sample patterned with standard lithographic process. The darker area corresponds to the sample surface. The position of the current and voltage terminals are indicated with I and V, respectively, whereas the black arrow indicates the strip.

contacts was L = 400 μm. No substantial changes in the *I-V* characteristics and resistivity values were observed for samples patterned with strip widths in the range 50–100 μm. The resistivity and *I-V* measurements were performed using the standard four-probe dc technique, where two of the in-line V terminals (V_1 and V_3 or alternatively V_2 and V_4) were used as voltage probes. For all the measurements, the current electrodes were attached at the left and right I labeled terminals and the current has been considered uniformly distributed along the sample thickness.

The Hall voltage V_H was measured between two of the opposite voltage terminals ($V_{H^{1-2}} = V_1 - V_2$ or alternatively $V_{H^{3-4}} = V_3 - V_4$) with the external magnetic field B perpendicular to the sample surface. In this case the strip width was 50 μm while the distance between two pairs of the in-line terminals was the same as for *I-V* measurements. During Hall voltage measurements, in order to reduce possible spurious effects due to sample and strip uniformity, the directions of the current and the magnetic field were inverted and V_H was measured between both the opposite voltage pairs for each value of B and I. The difference in the measured values of V_H in the different configurations resulted to be less than the experimental uncertainty.

X-ray absorption spectroscopy (XAS) experiment was performed at the beamline ID08 of the European Synchrotron Radiation Facility using the high scanning speed Dragon-type monochromator. The x-ray source was an Apple II undulator delivering almost 100% polarized radiation in both horizontal and vertical directions. The total electron yield detection had a probing depth of 3–6 nm, so that several superlattice cells under the surface could be investigated. The incident beam was forming a 60° angle with the sample surface normal, which is parallel to the crystal c axis. In this geometry, with vertical polarization the electric field vector **E** of the incident radiation was parallel to the ab-plane. With horizontal polarization **E** was mostly parallel to the c-axis, so that 75% of the intensity comes from the final states lying perpendicular to the ab-plane.

III. RESULTS AND DISCUSSION

In Fig. 3(a) the x-ray diffraction (XRD) spectrum of a superconducting SL $(CCO)_n/(STO)_m$, with nominal composition $n = 3$ and $m = 2$, reveals the presence of sharp satellite peaks around the average structure one, indicating the formation of a high quality superlattice with period $\Lambda \approx 19.5(5)$ Å, $n = 3.5(5)$, and $m = 2.0(5)$. To better evaluate the structural quality of CCO/STO SLs, we recorded a HRTEM image on an identical sample along the [110] direction of the $NdGaO_3$ substrate. The image [Fig. 3(b)] shows a heteroepitaxial superlattice film growth and a series of stacked layers with different contrast, regularly alternating thicknesses and sharp interfaces. The high quality of the SL is confirmed by the Fourier transform (FT) pattern [inset of Fig. 3(b)], where, beside the intense reflections associated with the CCO and STO substructures, satellite lower intensity reflections are observed in the growth direction (i.e., [001]* direction). These reflections are ascribed to the periodic structure generated by the regular stacking of CCO and STO. The stacking can be described as an average of 3.5 u.c. of CCO and 2 u.c. of STO, with a superlattice period $\Lambda \approx 19$ Å, in agreement with the

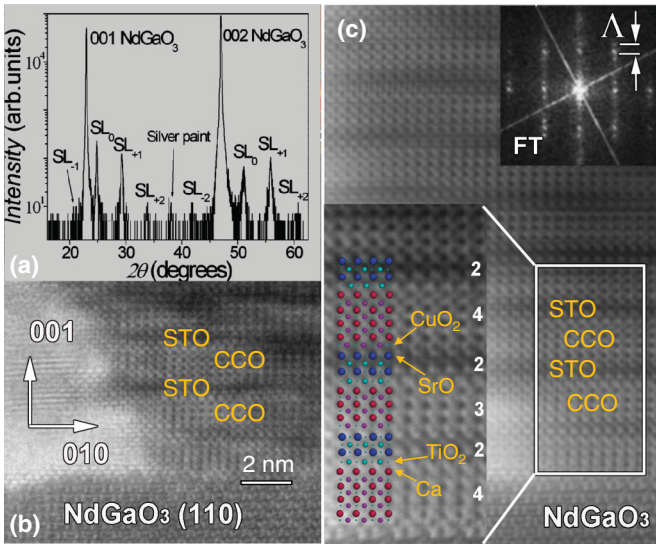

FIG. 3. (Color online) (a) XRD pattern (intensity in log scale) from $(CaCuO_2)_{3.5}/(SrTiO_3)_2$ SL. $SL_{\pm i}$ mark the satellite peaks, around the average structure peak SL_0. (b) HRTEM image of an identical SL taken along the [110] orientation of the $NdGaO_3$ substrate. (c) filtered HRTEM image. Bottom inset: enlargement of the area marked by white rectangle close to substrate with the atomic model of STO-CCO sequences (dark blue: Sr; light blue: Ti; small light blue: O; red: Ca; purple: Cu). Top inset: Fourier Transform pattern where superlattice spots are clearly visible along [001] growth direction.

XRD analysis. This means that the number of CCO u.c. varies from 3 to 4. This assignment is confirmed by the analysis of the filtered HRTEM image [see Fig. 3(c)], where it is possible to precisely determine the layers stacking, as illustrated in the colored circles model structure in the inset.

We have observed that the conductivity of $(CCO)_n/(STO)_m$ SLs slightly varies with varying n and m, but increases substantially with increasing the oxidizing power of the growth atmosphere, till the occurrence of superconductivity. In particular, for a weakly oxidizing growth atmosphere (oxygen pressure lower than 0.1 mbar) the SLs show always a semiconductorlike temperature dependence of the resistance [Fig. 4(c)], even if the film is quenched to room temperature in high (about 1 bar) oxygen pressure. An insulator to metal transition occurs only when a highly oxidizing growth atmosphere is used (oxygen plus 12% ozone at a pressure of about 1 mbar) and the film is rapidly quenched to room temperature at high oxygen pressure (about 1 bar). Under these conditions, the SL is metallic, and, in the best case, the resistance goes to zero at about 40 K [Fig. 4(c)]. Thus, strong oxidation is a key ingredient to obtain superconducting samples.

The occurrence of superconductivity has been also characterized by magnetization and critical current density (J_c) measurements. The temperature dependence of J_c was obtained by the measurement, on suitably patterned samples (see Fig. 2), of the *I-V* characteristics shown in Fig. 4(e) at different temperatures. To determine J_c at each temperature, a 1 μV criterion has been adopted [vertical dashed line in the inset of Fig. 4(e)]. At $T = 6$ K, $J_c = 1.1 \times 10^5$ A/cm^2, a value comparable with other superconducting SLs.[3] The magnetic moment was measured by means of a commercial

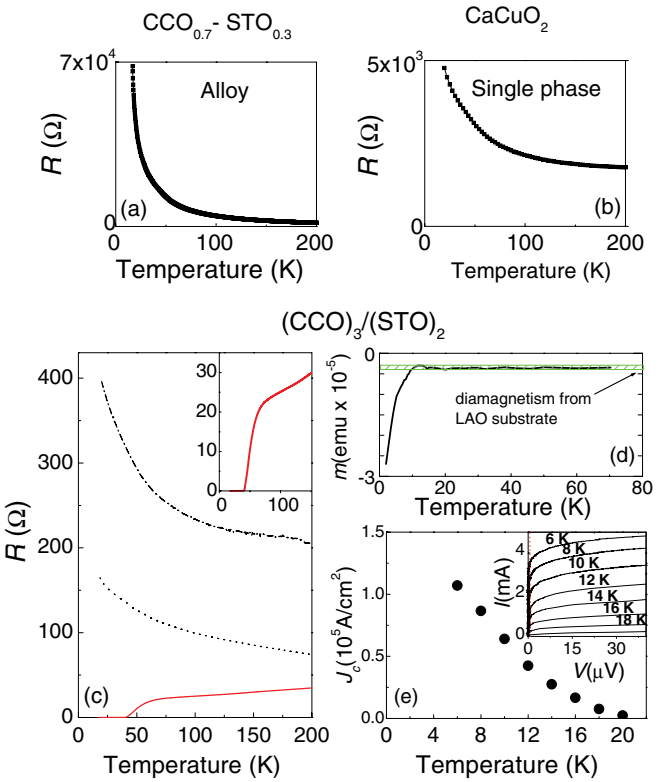

FIG. 4. (Color online) $R(T)$ of the CCO-STO alloy (panel a) and the single phase CCO (panel b) grown in the same conditions as the superconducting SLs. (c) $R(T)$ for a SL grown in low oxidizing atmosphere (dash-dotted line), for one grown in the same condition and quenched in high (about 1 bar) oxygen pressure (dotted line), and for a SL grown in a oxygen/ozone mixed atmosphere at higher pressure and quenched in high oxygen pressure (full line). Inset: superconducting transition shown on a reduced temperature range. (d) Magnetic moment as a function of temperature for a $(CCO)_3/(STO)_2$ SL grown on $LaAlO_3$ substrate. The horizontal green line indicates the value of the temperature independent diamagnetism of LAO. (e) Critical current density as a function of temperature for a SL with $T_c = 22$ K after patterning process. Inset: I-V characteristics at different temperature for the sample patterned as shown in Fig. 2. The vertical dashed line at $V = 1\mu V$ corresponds to the criterion adopted for I_c measurement.

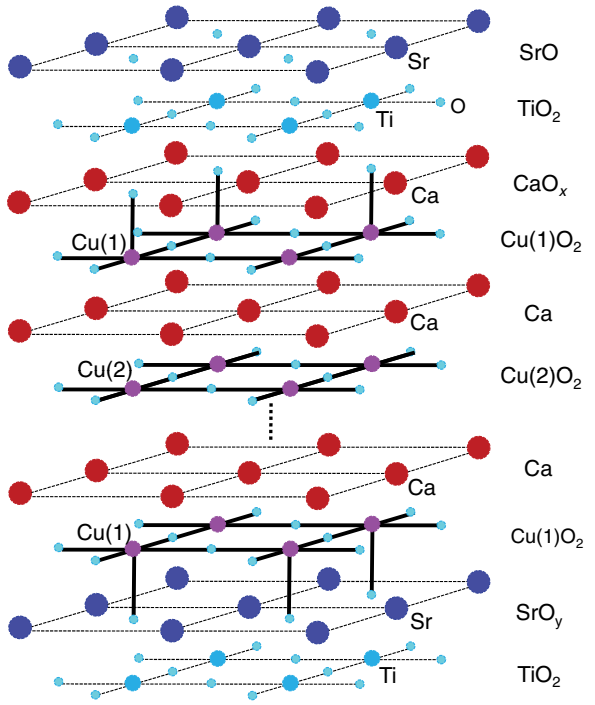

FIG. 5. (Color online) Schematic representation of the layered structure of the superlattice where the two Cu sites, Cu(1) and Cu(2) with different oxygen coordination, are shown. The thick full lines represent the coordination of Cu with O.

SQUID by Quantum Design. Since the NGO substrate is strongly paramagnetic,[18] and, at low temperature, it hinders the detection of the diamagnetic signal from the SL, then, as a substrate, we used $LaAlO_3$ (LAO), which has a small and temperature independent diamagnetism[19] [see Fig. 4(d)]. A clear signature of a diamagnetic transition in $(CCO)_3/(STO)_2$ SL does appear below 12 K. The T_c in this SL is much depressed compared to similar SLs grown on NGO, probably because of the larger and opposite in-plane lattice mismatch between LAO ($a = 3.78$ Å) and CCO ($a = 3.84$ Å).

Once proven the actual occurrence of a superconducting phase in CCO/STO SLs by transport and magnetization measurements, it is important now to point out that the proper doping and the consequent superconductivity do occur only in the presence of a layered structure with sharp interfaces. Indeed, we have grown, in the same strongly oxidizing conditions used for the superconducting SLs, a CCO-STO alloy (interface free), with 70% CCO and 30% STO, and a pure CCO film: both systems show a semiconductorlike temperature dependence of the resistance with no trace of superconductivity [see Figs. 4(a) and 4(b)]. Therefore, the *layered structure* is needed in order to obtain superconductivity, and we can thus argue that the excess oxygen atoms enter at the CCO/STO interfaces.

Indeed, there are two kinds of interfaces in CCO/STO SLs (see Fig. 5): CuO_2-Ca-TiO_2-SrO and Ca-CuO_2-SrO-TiO_2. Both the interfaces are hybrid between the perovskite and the IL structure. For instance, the first one could adopt the IL structure of $CaCuO_2$ (CuO_2-Ca-TiO_2-SrO) or the perovskite structure of $CaTiO_3$ (CuO_2-CaO-TiO_2-SrO), depending on the oxygen content at the interface Ca plane. Similarly, at the other interface we can have the IL $SrCuO_2$ or the perovskite $SrTiO_3$. Therefore, it is likely that the two interfaces have CuO_2-CaO_x-TiO_2-SrO and Ca-CuO_2-SrO_y-TiO_2 compositions. Under strongly oxidizing conditions, the overall oxygen content at the interfaces $(x + y)$ could become larger than one, giving rise to doping.

Since we expected that the doping occurs at the interface, we investigated how far from the interfaces superconductivity extends. To this aim we prepared a series of SLs, where the number of STO u.c. is kept fixed at $m = 2$ and the number of CCO u.c. is varied from $n \approx 1.5$ to $n \approx 20$ (see Sec. II A). Superconductivity shows up when n becomes larger than 2, and T_{cm}, defined as the transition midpoint in the $R(T)$ curves [inset to Fig. 6(a)], reaches the maximum value for n between 3 and 4 [Fig. 6(a)]. For higher values of n, T_{cm} decreases, and for $n > 5$ remains almost constant up to the thickest sample ($n \approx 20$). This behavior suggests that superconductivity is confined within a few unit cells from the interface. To further

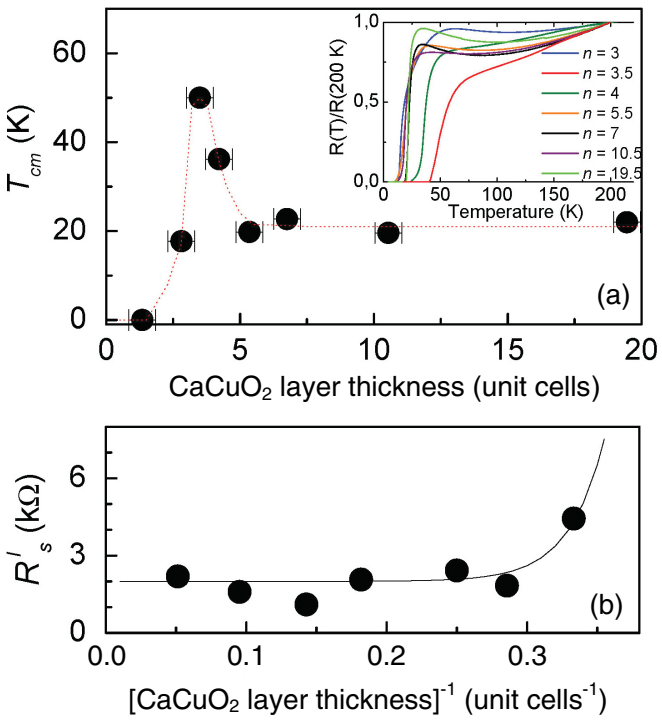

FIG. 6. (Color online) (a) T_{cm}, defined as the midpoint of the resistive transitions shown in the inset, as a function of the number n of unit cells of the CCO. The dotted line is a guide for the eye. Inset: $R(T)$ normalized at $T = 200$ K for the same SLs as in the main panel. (b) Sheet resistance at 80 K of one CCO layer R_s^l as a function of the inverse of the number of CCO unit cells. Full line is a guide to the eye.

confirm this conclusion, we analyzed the sheet resistance R_s multiplied by the number M of CCO layers within the superlattice (i.e., the number of repetitions of the CCO_n/STO_m supercell): $R_s^l = M \times R_s$, which is thus the sheet resistance per CCO layer. If the carriers were uniformly distributed over the whole CCO layer, R_s^l would depend linearly on the inverse of the number $n$of CCO unit cells in the layer, extrapolating to $R_s^l = 0$ at $n^{-1} = 0$. But this is not the case, since, as shown in Fig. 6(b), R_s^l does not appreciably vary with the CCO thickness, except for the SL with the thinnest CCO layer.

Given that superconductivity in CCO/STO SLs deals with the interface properties, it is worth mentioning here that at the CCO/STO interface a large polar discontinuity is present, since the planes TiO_2 and SrO of STO are neutral, whereas the planes Ca and CuO_2 of the CCO are charged ($+2e$ and $-2e$ per unit cell, respectively). Therefore, some sort of interface reconstruction should occur in order to suppress this huge built-in electrostatic potential. Most likely, a pure ionic mechanism involving displacement of oxygen ions, similar to the case of the interface between SrO terminated STO and LAO,[10] is at work in CCO/STO SLs, due to the hybrid (perovskite/infinite layer) interfaces, where the presence of a variable oxygen content is allowed.

We have up to now shown that: (i) it is possible to synthesize cuprate/titanate heterostructures with high structural quality; (ii) a high T_c superconducting phase does actually occur in these systems; (iii) sharp interfaces and strongly oxidizing growth conditions are needed to obtain superconductivity; (iv) (super)conductivity is confined within a few unit cells

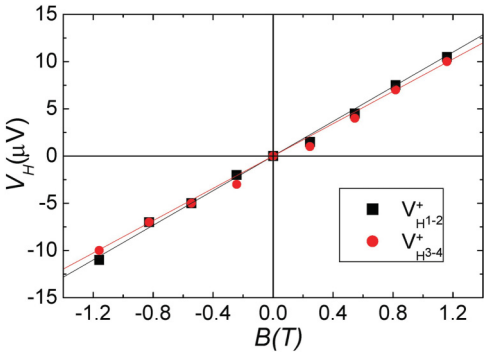

FIG. 7. (Color online) Hall voltage V_H as a function of magnetic field B for a given direction of the bias current fixed at $I = 0.1$ mA. Square and circles refers to V_H values acquired between terminals 1-2 and terminals 3-4, respectively, as indicated in the picture of the patterned sample (Fig. 2). The straight lines are linear fit to the data with the slope proportional to R_H.

from the interfaces. Therefore, the engineering of the synthetic heterostructure CCO/STO led to a new phase of electron matter, i.e., high T_c superconductivity, which does not exist in the single insulating constituent oxides, being exclusively a consequence of a process occurring at the interface between CCO and STO. To reach a deeper knowledge of the process operating at the interface, which involves the presence of excess oxygen ions, we performed additional key experiments, whose results are illustrated in the following. Hall voltage (V_H) measurements were performed on suitably patterned samples (see Fig. 2). V_H was measured at room temperature between the opposite voltage contacts biasing the sample with a 100 μA dc current and applying an external magnetic field B up to 1.2 T. In Fig. 7, V_H as a function of the external magnetic field B is shown for both the voltage configurations and for one direction of the current. For each configuration a Hall constant R_H is obtained by the slope of the best fit straight line through the experimental data. By the average of the calculated slopes of the different experimental data set (two opposite voltage terminals and two current directions), the value $R_H = 3.4 \times 10^{-3}$ cm^3/C was obtained. The positive sign of R_H gives a strong indication of the hole nature of the majority charge carriers in these materials. The calculated charge density is $n_H = 1.8 \times 10^{21}$ cm^{-3}, which results comparable with that observed in other cuprate superconductors and cuprate based SLs.[20]

One of the original characteristics of the CCO/STO SLs, with respect to other previously reported high T_c HSs,[1,3,22] is that in CCO/STO Cu is present only in one of the two constituent blocks. In this case a block selective study is possible by resonant spectroscopic techniques. We thus additionally performed x-ray absorption spectroscopy measurements.[21,22] Indeed, XAS is a well established synchrotron based technique providing chemical and site selective information on the electronic states close to the Fermi level. In highly correlated 3d transition metal systems $L_{2,3}$ edge XAS (mainly 2p→ 3d transitions) can reveal the symmetry of unoccupied 3d states and distinguish among sites with different valence and coordination. XAS spectra were collected at 5 K at the Cu and Ti $L_{2,3}$-edges[23] on a superconducting $(CCO)_3/(STO)_2$ SL with $T_c = 25$ K, and on an identical SL, but *non-superconducting*, since grown with no ozone and with no quenching at high

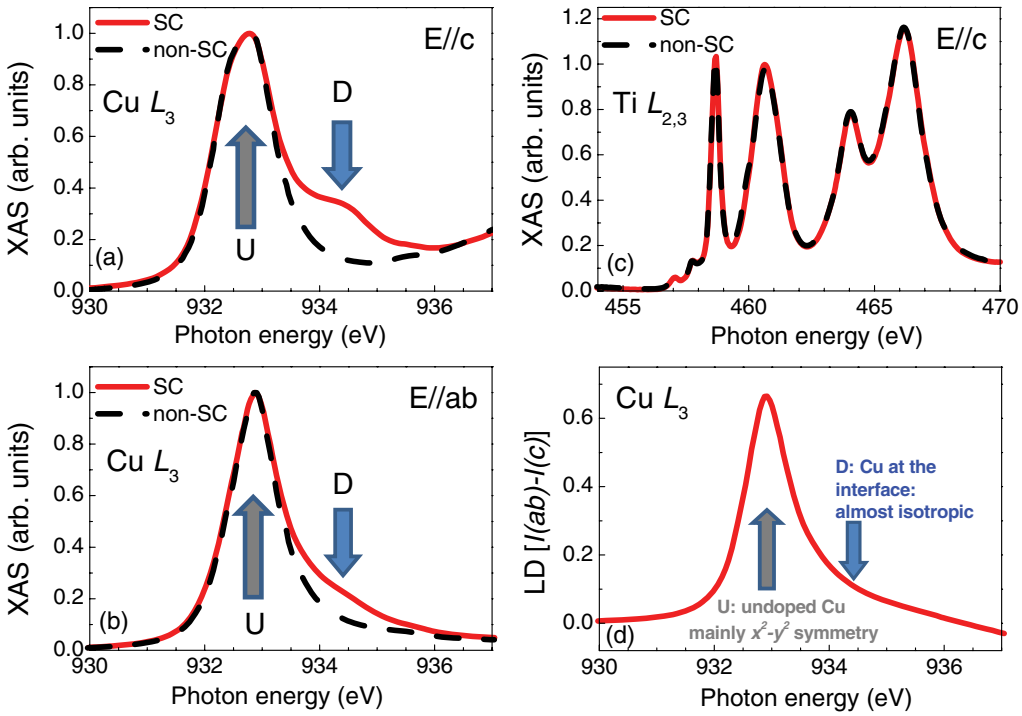

FIG. 8. (Color online) (a),(b): Cu L_3-edge for a superconducting (SC) (full line) and non-superconducting (dashed line) $(CCO)_3/(STO)_2$ SL. All measurements are performed at $T = 5$ K and the spectra are normalized to the maximum height intensity of the L_3 edge. (c) The two multiplets Ti L_2- and Ti L_3-edges for SC and non-SC sample. (d) Linear dichroism for the SC sample.

oxygen pressure. A linear background was fitted to the pre-edge region of the L_3 edge and subtracted from the spectra, which are then normalized to the edge jump set to unity above the L_2 edge. Figures 8(a) and 8(b) show the normalized XAS spectra taken at the Cu L_3-edge (Cu $2p \rightarrow$ Cu $3d$ electron transition energy) for the two samples, with the electric field of the incident radiation parallel to the c axis ($\mathbf{E} \parallel c$) and to the ab plane ($\mathbf{E} \parallel ab$), respectively. The L_3 peak at 932.8 eV, indicated with U in Fig. 8, is associated with the process in which the $3d^9$ ground state becomes $c3d^{10}$ ($3d^9 \rightarrow c3d^{10}$), where c indicates a Cu 2p core hole. This peak is assigned to the absorption by an undoped Cu site.[22,24,25] The feature indicated with D at about 1.5 eV above the main peak U is associated with the process $3d^9\underline{L} \rightarrow c3d^{10}\underline{L}$, where $\underline{L}$ indicates an additional oxygen ligand hole arising from Cu $3d$ – O $2p$ hybridization, mainly with an O $2p$ character.[21,22,24] Thus, this feature is assigned to the absorption by doping holes.[22,24,25] The major differences between the spectra of superconducting and non-superconducting SL are observed in the region around D. In both polarizations, this region acquires spectral weight in the case of superconducting SL, as a clear indication of increased holes concentration delocalized on the in-plane and out-of-plane O $2p$ bands. We note here that the presence of out-of-plane ligand holes has been already observed in some HTS[26,27] and the debate about their role in superconductivity is still open. On the other hand, at the Ti $L_{2,3}$-edges, no relevant changes are observed between the superconducting and the non-superconducting samples [Fig. 8(c)]. According to Ref. 28, in case of Ti^{3+} doping, an increase of the intensity would be expected in the region between the peak at 464 eV, associated to the $3d$-t_{2g} final states, and the peak at 466 eV, associated to the $3d$-e_g final state. This increase, in our case, does not occur. Therefore, not only the valence, but also the crystal field in the Ti environment[28] are not substantially affected by the strongly oxidizing conditions used to obtain the superconducting sample. Thus, by a direct observation of the XAS spectra we have confirmed that the charge carriers are holes and established that they are located in the CCO block.

With the help of the Cu-L_3-edge linear dichroism (LD) shown in Fig. 8(d), a more detailed comprehension of the XAS spectral features can be obtained. The XAS LD [Fig. 8(d)] is the difference between the XAS contributions from the two polarizations: $\mathrm{LD} = I(\mathbf{E} \parallel ab) - I(\mathbf{E} \parallel c)$, where both spectra have been normalized to the value of the L_3 intensity of the $\mathbf{E} \parallel ab$ spectrum. LD is thus a measure of the anisotropy of the environment around selected ions. In the SLs CCO/STO we can distinguish two distinct Cu sites (see Fig. 5): (i) Cu(1) sites at the CuO_2 planes closest to STO (interface sites), which can have apical oxygen; (ii) Cu(2) sites at all the other CuO_2 planes, all of them with purely planar oxygen coordination. Upon doping (strong oxidization), the majority of Cu(1) sites are expected to have an apical oxygen because of additional oxygen atoms entering the interface planes. Since the c axis of CCO is about 3.19 Å, the out-of-plane Cu(1)-O distance (see Fig. 5) is not much different from the in-plane one, as it has been also shown in the doped CCO with planar defects.[13] Therefore, an isotropic orbital population is expected at Cu(1) sites. Recalling that the main peak U is ascribed to the absorption by undoped Cu sites and the region D to the absorption by delocalized doping holes, we can assign D, which is just weakly anisotropic (low LD), to the doped Cu(1) sites with both in-plane ($3d_{x^2-y^2}$) and out-of-plane ($3d_{3z^2-r^2}$) orbitals hybridized with oxygen orbitals. On the other hand,

the presence in the XAS spectra of spectral weight with large LD in the region about 1 eV above U [see Fig. 5(d)], can be ascribed to the absorption by doping holes with mostly in-plane $3d_{x^2-y^2}$ character[29] at the Cu(2) sites, which have purely planar oxygen coordination. We can thus conclude that the doping holes, although mainly confined at the Cu(1) sites, can get transferred to the neighboring Cu(2)O_2 planes, giving rise to an interfacelike superconductivity.

IV. SUMMARY

In summary, we synthesized the superconducting heterostructure $(CaCuO_2)_n/(SrTiO_3)_m$, with maximum T_c = 40 K, by alternating an insulating IL cuprate (CCO) and a copper-free wide gap semiconductor (STO). The charge reservoir role is played by the interfaces, due to the peculiar structural and electronic properties of the constituent oxides, which allow extra oxygen ions entering the interface planes. The doping holes, from the interface layers, are injected in the inner CuO_2 planes close to the interface, whereas STO does not contribute to transport. This work could motivate the search for other cuprate/noncuprate synthetic heterostructures, in which the CuO_2 plane properties (in-plane Cu-O distance, buckling), the charge reservoir characteristics, and the out-of plane unit cell size can be independently controlled. This possibility may lead to improved superconducting properties of the HSs and to unveil open questions concerning superconductivity in cuprates.

ACKNOWLEDGMENTS

W.P. and O.I.L. are grateful to A. Pautrat for helpful discussion and to M. L. Gouleuf for the preparation of the samples for HRTEM measurements. D.D.C. thanks A. Maisuradze for support during magnetization measurement. C.A. and D.D.C. thank J. Zeghenagen for fruitful discussions. This work was partly supported by the Italian MIUR (Grant No. PRIN-20094W2LAY, "Ordine orbitale e di spin nelle eterostrutture di cuprati e manganiti").

[1] G. Balestrino, S. Martellucci, P. G. Medaglia, A. Paoletti, and G. Petrocelli, Phys. Rev. B **58**, R8925 (1998).
[2] G. Balestrino, G. Pasquini, and A. Tebano, Phys. Rev. B **62**, 1421 (2000).
[3] A. Gozar, G. Logvenov, L. Fitting Kourkoutis, A. T. Bollinger, L. A. Giannuzzi, D. A. Muller, and I. Bozovic, Nature (London) **455**, 782 (2008).
[4] N. Reyren, S. Thiel, A. D. Caviglia, L. Fitting Kourkoutis, G. Hammerl, C. Richter, C. W. Schneider, T. Kopp, A.-S. Rüetschi, D. Jaccard, M. Gabay, D. A. Muller, J.-M. Triscone, and J. Mannhart, Science **317**, 1196 (2007).
[5] N. Ya. Fogel, E. I. Buchstab, Yu. V. Bomze, O. I. Yuzephovich, M. Yu. Mikhailov, A. Yu. Sipatov, E. A. Pashitskii, R. I. Shekhter, and M. Jonson, Phys. Rev. B **73**, 161306 (2006).
[6] F. M. Muntyanu, A. Gilewski, K. Nenkovb, A. Zaleski, and V. Chistol, Solid State Commun. **147**, 183 (2008).
[7] J. Barzola-Quiquia, J.-L. Yao, P. Rödiger, K. Schindler, and P. Esquinazi, Phys. Status Solidi A **205**, 2924 (2008).
[8] C. Cen, S. Thiel, J. Mannhart, and J. Levy, Science **323**, 1026 (2006).
[9] E. Dagotto, Science **318**, 1076 (2007).
[10] N. Nakagawa, H. Y. Hwang, and D. A. Muller, Nat. Mater. **5**, 204 (2006).
[11] T. Siegrist, S. M. Zahurak, D. W. Murphy, and R. S. Roth, Nature **334**, 231 (1988).
[12] M. Azuma, Z. Hiroi, M. Takano, Y. Bando, and Y. Takeda, Nature (London) **356**, 775 (1992).
[13] H. Zhang, Y. Y. Wang, H. Zhang, V. P. Dravid, L. D. Marks, P. D. Han, D. A. Payne, P. G. Radaelli, and J. D. Jorgensen, Nature (London) **370**, 352 (1994).
[14] S. Tao and H.-U. Nissen, Phys. Rev. B **51**, 8638 (1995).
[15] G. Balestrino, R. Desfeux, S. Martellucci, A. Paoletti, G. Petrocelli, A. Tebano, B. Mercey, and M. Hervieu, J. Mater. Chem. **5**, 1879 (1995).
[16] T. Ohnishi, K. Takahashi, M. Nakamura, M. Kawasaki, M. Yoshimoto, and H. Koinuma, Appl. Phys. Lett. **74**, 2531 (1999).
[17] I. K. Schuller, M. Grimsditch, F. Chambers, G. Devane, H. Vanderstraeten, D. Neerinck, J.-P. Locquet, and Y. Bruynseraede, Phys. Rev. Lett. **65**, 1235 (1990).
[18] A. Podlesnyak, S. Rosenkranzt, F. Fauthi, W. Martit, A. Furrert, A. Mirmelsteint, and H. J. Scheels, J. Phys.: Condens. Matter. **5**, 8973 (1993).
[19] M. Khalid, A. Setzer, M. Ziese, P. Esquinaz, D. Spemann, and A. Pöppl, Phys. Rev. B **81**, 214414 (2010).
[20] M. Affronte, J.-M. Triscone, O. Brunner, L. Antognazza, L. Miéville, M. Decroux, and Ø. Fischer, Phys. Rev. B **43**, 11484 (1991).
[21] J. Fink, N. Nücker, E. Pellegrin, H. Romberg, M. Alexander, and M. Knupfer, Electron Spectrosc. Relat. Phenom. **66**, 395 (1994).
[22] C. Aruta, G. Ghiringhelli, C. Dallera, F. Fracassi, P. G. Medaglia, A. Tebano, N. B. Brookes, L. Braicovich, and G. Balestrino, Phys. Rev. B **78**, 205120 (2008).
[23] F. M. F. de Groot, J. C. Fuggle, B. T. Thole, and G. A. Sawatzky, Phys. Rev. B **41**, 928 (1990).
[24] A. Bianconi, A. Congiu Castellano, M. De Santis, P. Rudolf, P. Lagarde, A. M. Flank, and A. Marcelli, Solid State Commun. **63**, 1009 (1987).
[25] D. D. Sarma, O. Strebel, C. T. Simmons, U. Neukirch, G. Kaindl, R. Hoppe, and H. P. Muller, Phys. Rev. B **37**, 9784 (1988).
[26] P. Srivastava, B. R. Sekhar, C. Gasser, F. Studer, K. B. Garg, C. T. Chen, and M. Pompa, J. Phys.: Condens. Matter **10**, 3417 (1988).
[27] R. K. Singhal, S. Dalela, D. Chaturvedi, B. Dalela, N. L. Saini, B. R. Sekhar, K. B. Garg, V. Beaumount, B. Mercey, C. T. Chen, Hong-Ji Lin, and T. Y. Huo, J. Phys.: Condens. Matter **13**, 6865 (2001).
[28] J. Verbeeck, S. Bals, A. N. Kravtsova, D. Lamoen, M. Luysberg, M. Huijben, G. Rijnders, A. Brinkman, H. Hilgenkamp, D. H. A. Blank, and G. Van Tendeloo, Phys. Rev. B **81**, 085113 (2010).
[29] C. T. Chen, L. H. Tjeng, J. Kwo, H. L. Kao, P. Rudolf, F. Sette, and R. M. Fleming, Phys. Rev. Lett. **68**, 2543 (1992).